

# Selective Adsorption on Fluorinated Plastic Enables the Optical Detection of Molecular Pollutants in Water

R. Lanfranco<sup>a</sup>, F. Giavazzi<sup>a</sup>, M. Salina<sup>b</sup>, G. Tagliabue<sup>a</sup>, E. Di Nicolò<sup>c</sup>, T. Bellini<sup>a</sup>, M. Buscaglia<sup>a</sup>

<sup>a</sup> Dipartimento di Biotecnologie Mediche e Medicina Traslazionale, Università degli Studi di Milano, 20090 Segrate, Italy;

<sup>b</sup> Proxentia S.r.l., 20135 Milano, Italy;

<sup>c</sup> Solvay Specialty Polymers, 20021 Bollate (MI), Italy

## Abstract

Amorphous fluorinated plastic can be produced with a refractive index similar to that of water, a condition that makes it essentially invisible when immersed in aqueous solutions. Because of this property, even a small amount of adsorbed molecules on the plastic-water interface provides a detectable optical signal. We investigated two distinct substrates made of this material, characterized by different interface area: a prism and a newly realized micro-porous membrane. We demonstrate that both substrates enable the label-free detection of molecular compounds in water even without any surface functionalization. The adsorption of molecules on the planar surface of the prism provides an increase of optical reflectivity, whereas the adsorption on the internal surface of the micro-porous membrane yields an increase of scattered light. Despite the different mechanisms, we found a similar optical response upon adsorption. We confirmed this result by a theoretical model accounting for both reflection and scattering. We investigated the spontaneous adsorption process for different kinds of molecules: surfactants with different charges, a protein (lysozyme) and a constituent of gasoline (hexane). The measured equilibrium and kinetic constants for adsorption differed by orders of magnitudes among the different classes of molecules. By suitable analytical models, accounting for the effects of mass limitation and transport, we found a simple and general scaling of the adsorption parameters with the molecular size.

## I. INTRODUCTION

The widespread availability of autonomous analytical devices enabling the real-time monitoring of a large number of sensible environmental parameters represents a futuristic scenario that is largely desirable but still far from practical realization. Over the past decades, a large effort has been devoted to the development of innovative molecular sensors and many promising technical solutions have been delivered [1][2]. However, very few of these have been brought out of the laboratory and exploited in the realization of devices capable of sustaining the harsh conditions of environmental monitoring sites. The requirements for deployable autonomous systems include operational simplicity of the measurement, limited instrumental complexity, minimum cost of the

device, high reusability and resistance to chemical, biological and physical stresses. These features are not easily combined in a single device that also must provide high detection performance. In the context of analytical laboratories, where the conditions are more favorable, colorimetric methods, infrared spectroscopy [3], liquid chromatography and mass-spectroscopy [4][5] are widely employed approaches to detect contaminants in liquids and solubilized media. However, the most common and widespread techniques to detect surfactants or oily compounds in water require the collection of suitable amounts of sample and preparation steps performed by highly specialized personnel in furnished laboratories [6]. Therefore, these techniques are typically expensive and time consuming. Innovative nano-structured materials [7], novel electrochemical transducers [8] and engineered biomolecular probes [9] may also provide improved detection performance in the controlled lab conditions. Nevertheless, all these approaches have so far failed to match all the requirements for an inexpensive deployable system.

Recent works have shown how the peculiar optical properties of certain amorphous perfluorinated polymer materials can be exploited to realize sensitive label-free biosensors based on simple components and requiring minimum sample processing[10][11]. In particular, amorphous copolymers of tetrafluoroethylene can be realized in order to present high transparency and a refractive index very close to that of water [12]. These materials become barely visible when immersed into an aqueous solution. Various surface treatments were developed to immobilize specific bio-receptors on their surface. This enabled to detect the binding of different bio-molecular targets through the increase of the light scattered by suspended nano-particles[13][14][15] or reflected by the surface of a prism [10][16]. Despite the high performance for biomolecular detection, these systems presented a few drawbacks that limited their exploitation in autonomous deployable platforms for on-line monitoring applications, possibly to be performed in harsh environments. In particular, the suspension of nano-particles provides the advantage of a large sensing surface that facilitates the detection of small molecules in abundant sample volumes. However, the particles can form aggregates that complicate the analysis of the light scattering signal. Additionally, the suspension format is not suitable for a continuous use in fluidic circuits. In contrast, the planar reflective surface of the prism provides an ideal support for fluidic integration. However, in the previous studies, the surface immobilization of specific bio-molecular probes was required to provide the binding and therefore the detection. Consequently, the flexibility of measuring conditions, the reusability and the storage of the sensing substrates are generally limited by the necessity to preserve the full functionality of the bio-molecular recognition elements.

On the other hand, the index-matched perfluorinated substrates, when used as optical sensing materials, provide peculiar and interesting features, still largely unexplored: (i) Their surface in aqueous environment is at the same time hydrophobic and negatively charged, and induces the spontaneous adsorption of various molecular compounds; (ii) They exhibit a high resistance to chemical and biological stresses and, therefore, they can be easily cleaned and regenerated [17][18]; (iii) Substrates with different shapes and structures down to the micron-scale can be easily realized using conventional fabrication processes for plastic materials [19]. In principle, the spontaneous adsorption of different molecular compounds mentioned in (i) can be exploited to detect contaminants in aqueous solutions. However, the possible selectivity of the adsorption process onto index-matched perfluorinated plastics is largely undetermined. Previous studies on the electrokinetic properties of rod-like colloids made of crystalline polytetrafluoroethylene have addressed the characterization of surfactant adsorption to control the surface charge of the particles

[20][21]. More generally, the formation of an adsorbed molecular layer at the solid-liquid interface may represent a complex process, potentially involving various morphological rearrangements and different time-scales [22][23][24][25][26][27][28][29][30]. Kinetics measurements are increasingly used to gain a deeper understanding of these phenomena [23]. Nevertheless, simple theoretical models suitable to predict the behavior of different classes of molecules are not yet available. In the case of surfactants, most studies have focused on the adsorption behavior at relatively high concentrations across the critical micelle concentration (CMC). In contrast, in order to design novel sensitive detection systems, suitable characterization and modeling of the adsorption process at the lowest detectable concentrations are required.

Here we present a new concept of optical detection systems based on perfluorinated materials iso-refractive with water. We realized a right angle prism suitable for reflection measurements and a micro-porous membrane for light scattering measurements. The presence of surfactants in solution yielded an increase of the intensity of light reflected by the prism or scattered by the membrane due to the adsorption on their surface. We characterized the adsorption process at equilibrium for both systems. Remarkably, a common optical model accounts for both the reflection from the prism and the light scattered from the membrane upon adsorption of molecules. Through this model, the optical signals were converted into the thickness of the molecular layer formed at the interface, which was found to be in agreement with the size of the molecules. We obtained a detailed description and characterization of the adsorption process for different molecules by means of the prism system. Surfactants with different net charge, hexane and the protein lysozyme spontaneously adsorbed providing different signals. Remarkably, both the equilibrium constants for adsorption and the kinetic parameters differed by order of magnitudes among the three classes of molecules. Overall, simple adsorption and transport models enabled to identify structural features related to the molecular size as important parameters affecting the adsorption process. These results indicate the possibility of different adsorption fingerprints enabling to discriminate among different molecular compounds in aqueous samples and, therefore, provide the basis for a new class of sensing materials, potentially suitable for on-line detection instruments with very low complexity.

The following sections are organized in this way: In Section II we introduce the prism and membrane sensing substrates and propose a common optical model accounting for their signal upon adsorption; In Section III we compare the response to different concentrations of surfactant for the two systems by a simple adsorption model; In Section IV we compare the adsorption at equilibrium for different classes of molecules on the prism sensor and discuss the observed dependence of the adsorption strength on the molecular size; In Section V the adsorption kinetics observed for the different molecules are interpreted considering diffusion and transport effects, which also scale with the molecular size. Section VI reports a summary of the main results.

## **II. OPTICAL SIGNAL FROM REFLECTANCE AND SCATTERING MEASUREMENTS**

In this Section we describe two different sensing substrates index-matched with water: a prism and a newly realized micro-porous membrane. The adsorption of molecules at their interface yields an increase of reflected or scattered light intensity, respectively. For both systems, the signal increase is ascribed to the formation of a thin layer of different refractive index separating the solid and liquid media with similar refractive indices. We show that, in this index-matching condition and

for a thickness  $h$  of the adsorbed layer much smaller the wavelength of light  $\lambda$ , the reflected or scattered intensity  $I$  is related to the amount of adsorbed molecules by simple optical models. More generally, other well-established techniques enable the characterization of the structure of a thin molecular layer on a planar surface by detailed modeling of the spectrum and polarization of the reflected light [31][32]. In this work we exploit a different approach: we simply measure the increase of reflected or scattered intensity of monochromatic light upon formation of the layer. We describe the quantity of adsorbed molecules through an effective thickness  $h$  that represents the thickness of an ideal homogenous layer with fixed refractive index  $n_l$ . For each compound, the value of  $n_l$  corresponds to the refractive index of a compact molecular layer and the extracted thickness  $h$  is proportional to the amount of adsorbed molecules. By this simplified model, we derive a scaling of either the reflected or scattered intensity with  $h^2$ . The general formula to account for the intensity signal  $I$  in the presence of the adsorbed layer relative to the intensity  $I_0$  measured in the absence of the layer is given by:

$$\frac{I}{I_0} = 1 + \left(\frac{h}{h^*}\right)^2 \quad (1)$$

where the value of the parameter  $h^*$  corresponds to the layer thickness yielding to  $I = 2I_0$  and, therefore,  $1/h^*$  represents the sensitivity of the optical response to molecular adsorption. Knowing the value of  $h^*$ , Equation 1 enables to convert the relative increase of reflected or scattered light intensity  $I/I_0$  into the effective thickness  $h$  of the adsorbed molecular layer. Remarkably, we show that, despite the different optical mechanism and the different area of the adsorbing interface, the values of  $h^*$  for the prism sensor and for the micro-porous membrane are substantially identical.

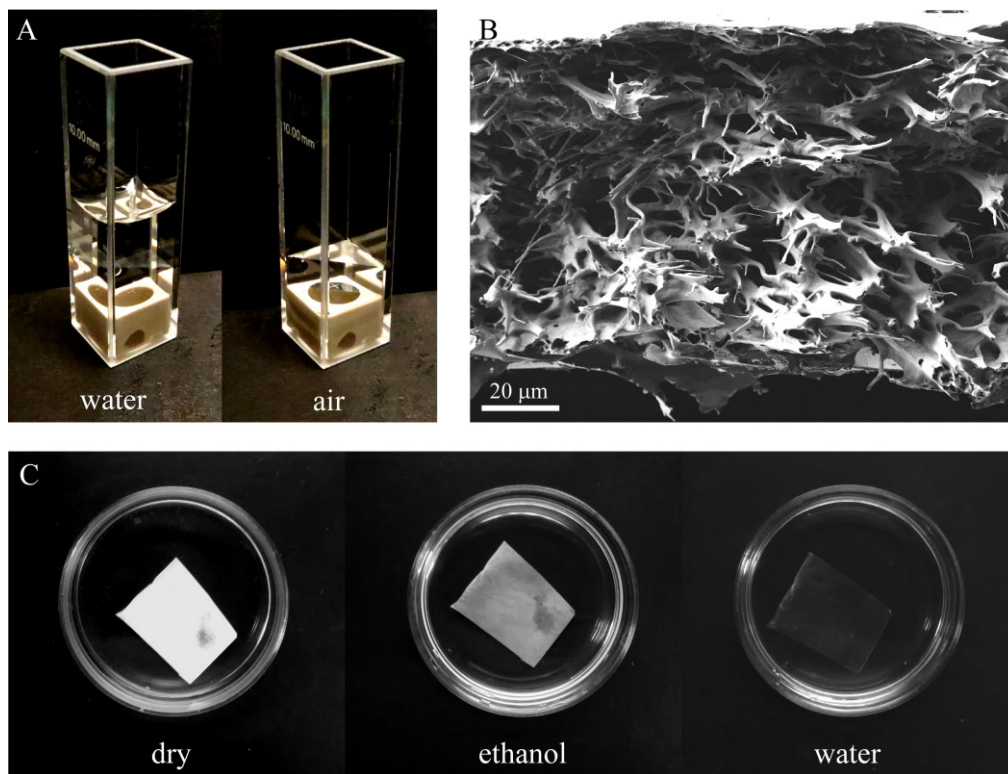


**Figure 1.** Perfluorinated materials isorefractive with water. (A) Images of a prism of Hyflon® AD immersed in water and in air, as indicated. (B) Electron microscope image (SEM) of the cross section of the membrane of Hyflon® AD. (C) Images of the same membrane immersed in water or ethanol and in air, as indicated.

## Prism sensor

Mechanical machining, printing and molding are common approaches for plastic manufacturing, which also apply to perfluorinated polymers. Prisms of Hyflon® AD (Solvay Specialty Polymers, Bollate, Italy) were previously produced by cutting and polishing and exploited for optical bio-sensing applications [10]. In this study, we used a similar prism without any surface coating or functionalization in order to detect and quantify the spontaneous adsorption of molecules on its planar surface. The prism was inserted in a 1-cm cuvette as show in Figure 1A. When immersed in water, the prism became barely visible. The adsorption of molecules with refractive index different from that of water provided a clear increase of reflected light intensity that was measured by a simple optical set-up, composed by a He-Ne laser and a photodiode. The cuvette hosting the prism also contained a stir bar, which provided the rapid mixing of the solution.

Amphiphilic compounds represent a suitable class of molecules to test the optical response to adsorption. Figure 2A reports the intensity of reflected light measured after the addition in solution of increasing concentrations of the cationic surfactant benzyldimethylstearylammmonium chloride monohydrate (SBSAC). The data refer to the equilibrium value of reflectivity measured about 500 s after the addition. A continuous increase of reflectivity was observed until a saturation was reached at high concentration, corresponding to the full coverage of the prism surface.

From the Fresnel formulas for thin film reflection [33], the measured value of reflectivity can be related to the thickness  $h$  of the layer formed by the adsorbed material [10]. For values of  $h$  up to dozens of nanometers, the reflected intensity  $I_R$  scales with  $h^2$  in agreement with Equation 1, where

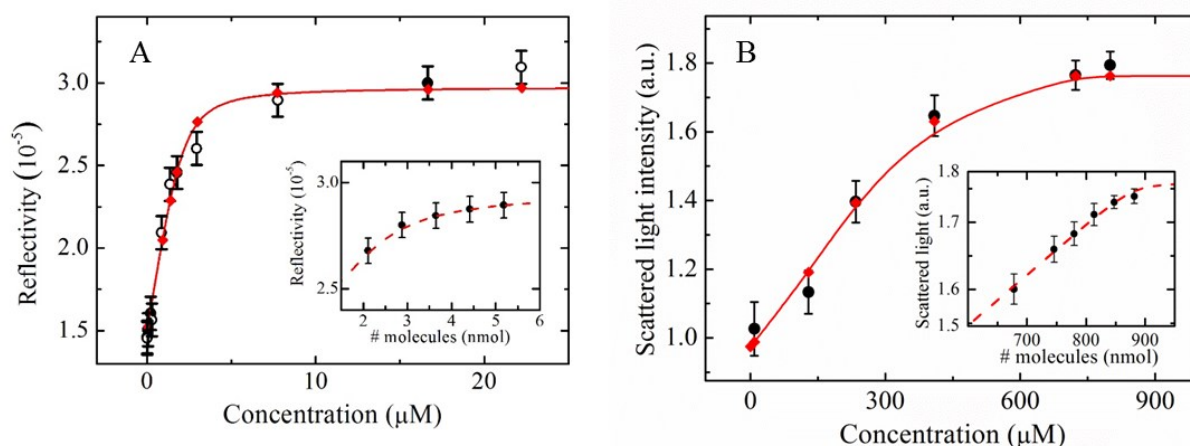


**Figure 2.** Adsorption of surfactant on different perfluorinated substrates index-matched to water. (A) Intensity of light reflected by the surface of the prism of Hyflon® AD for different concentrations of SBSAC in deionized water. At each addition, the sample volume in cuvette was increased by 100  $\mu\text{L}$ . Full and open dots refer to data from different experiments. Diamonds represent the value extracted from the fit as a function of  $C_0$  and  $V$ . The line is a spline to guide the eye. Inset: reflected intensity as a function of the sample volume for a constant concentration of 1.92  $\mu\text{M}$  (dots) and fitting curve (dashed line). (B) Intensity of light scattered by the micro-porous membrane of Hyflon® AD for different concentrations of SBSAC in deionized water. Dots and diamonds refer to experimental data and fitting value, respectively. The line is a spline to guide the eye. Inset: scattered light intensity as a function of the quantity of molecules in cuvette for a constant concentration of 340  $\mu\text{M}$  (dots) and fitting curve (dashed line).

$I = I_R$ , and  $I_0$  represents the intensity reflected by the bare surface. For small differences between the refractive indices of the solution and the solid material,  $n_s$  and  $n_m$ , respectively, the value of  $h^*$  is given by:

$$h^* = \frac{\lambda}{4\pi} \frac{\delta}{\bar{n}(\Delta - \frac{\delta}{2})} \left(1 - \frac{\Delta}{2\bar{n}}\right) \cos(\theta_i)^{-1} \quad (2)$$

where  $\bar{n} = (n_s + n_m)/2$ ,  $\delta = |n_s - n_m|$ ,  $\Delta = n_l - \bar{n}$ ,  $n_l$  is the refractive index of the adsorbing layer, and  $\theta_i$  is the angle of incidence relative to the surface normal. Compounds with different refractive index  $n_l$  yield to different values of  $h^*$  according to Equation 2. For the materials and the geometry exploited in this study and in the case of adsorption of SBSAC on the prism surface,  $h^* = 3.1$  nm. Consequently, the saturation value of reflectivity at high concentration reported in Figure 2A corresponds to a thickness  $h_{\max}$  of about 3 nm, in agreement with the molecular size of the surfactant, as further discussed below.

### Micro-porous membrane

Specifically designed methods are typically required to produce substrates with 3-dimensional microstructures, such as micron-size pores [34]. Here we report for the first time the realization of a micro-porous membrane made by Hyflon® AD, the same perfluorinated material used for the prism. The membrane was produced by non-solvent induced phase separation, as described in Appendix A. In the context of small molecule detection, as in the case of environmental monitoring applications, flow-through systems with high internal surface are expected to enhance the detection signal and the capture efficiency. A SEM image of a membrane with a thickness of about 100  $\mu\text{m}$  is reported in Figure 1B. The internal structure was qualitatively similar to that of commercially available membrane filters realized with more conventional materials [35][36]. Interconnected pores with the size of a few microns were present. The macroscopic optical appearance of the membrane strongly depended on the refractive index of the liquid filling the pores. As shown in Figure 1C, the membrane appeared white when completely dried, rather opaque when soaked with ethanol and transparent in water. The measured turbidity of the membrane in water was as low as 1.2  $\text{mm}^{-1}$ , meaning that more than 90% of the incident photons were not affected by scattering.

Figure 2B reports the scattered light intensity measured at an angle of 30° while illuminating the perfluorinated membrane with a diode laser at 532 nm (Coherent Compass 315M-100). The membrane was mounted on a rigid frame and immersed into a 1-cm cuvette. The mixing of the solution was provided by a magnetic stirring bar. The scattering signal increased rapidly after the addition of the surfactant SBSAC to the water solution and reached an equilibrium value in a few seconds. Figure 2B reports such equilibrium values measured about 500 s after the addition. The scattered light intensity increased as a function of the surfactant concentration until reaching a plateau corresponding to the full coverage of the membrane surface.

## Optical signal from the micro-porous membrane

We estimated the dependence of the light scattering signal on molecular adsorption by a simple model. We considered the intensity of scattered light for a collection of independent spherical particles with radius  $R$  and with refractive index  $n_m$  close to that of the surrounding solution,  $n_s$ . In general, the same calculation can be extended to particles of any shape characterized by some effective size  $2R$ . We considered the theoretical framework of the Rayleigh-Gans (RG) approximation [37], whose validity for nearly index-matching conditions extends to rather large values of  $R$ . Following the approach described in [38], we computed the intensity  $I_s$  of light scattered by the particles coated with a thin layer with refractive index  $n_l$  and thickness  $h \ll R$ . In the limit of small values of the thickness  $h$ , we obtain:

$$I_s = C \left\{ (n_m^2 - n_s^2) * \mathcal{F} + (n_l^2 - n_s^2) \frac{d\mathcal{F}}{dR} * h \right\}^2 \quad (3)$$

where  $C$  is a constant that depends on the number of particles and on the experimental set-up. The function  $\mathcal{F}$  is given by

$$\mathcal{F} = \int_V e^{i\mathbf{k} \cdot \mathbf{r}} dV \quad (4)$$

where  $V$  is the particle volume,  $\mathbf{k}$  is the scattering vector and  $\mathbf{r}$  is the vector indicating the position in space of the volume  $dV$ . In the limit of small particles ( $kR \ll 1$ ),  $\mathcal{F} = V$  up to a phase factor and the behavior previously observed for nanoparticles iso-refractive to water is recovered [13]. In this case, the light scattering increment  $I_s/I_0$  relative to the intensity scattered by the bare particles is also described by Equation 1 with  $I = I_s$ , assuming an even distribution of solid particles in solution and solution droplets embedded in the solid matrix, in order to account for the presence of convex and concave surface regions, respectively. Accordingly, for small spherical particles, the value of the parameter  $h^*$  is given by:

$$h^* = \left| \frac{n_m^2 - n_s^2}{n_l^2 - n_s^2} \right| \frac{R}{3} \quad (5)$$

As expected, smaller particles provide a higher relative increment of scattered light due to the coating layer, and the sensitivity scales linearly with the radius  $R$  [13].

A different scenario is expected for large particles ( $kR \gg 1$ ). However, a unifying model enabling to compare the optical response of a scattering system with that of the reflective surface was missing. Remarkably, we found that the simple RG framework is suitable to perform this evaluation. We considered a system of large particles and computed the average intensity of scattered light over a distribution of  $R$  with width  $\Delta R$ . We assumed a polydispersity of sizes such that  $k\Delta R \gg 1$ . This enabled to neglect the linear term  $\langle \mathcal{F} \frac{d\mathcal{F}}{dR} \rangle$  obtained from Equation 3, because  $\frac{d\mathcal{F}}{dR}$  and  $\mathcal{F}$  are both oscillating quantities as a function of  $R$  and they are in quadrature of phase, so the mean value of their product is equal to zero. Accordingly, a dependence of  $I_s$  on  $h^2$  is recovered and the relative increment of scattered light due to the coating layer is given in general by:

$$\frac{I_s}{I_0} = 1 + \left( \frac{n_l^2 - n_s^2}{n_m^2 - n_s^2} \right)^2 \frac{\langle dF^2 \rangle}{\langle F^2 \rangle} h^2 \quad (6)$$

In the limit of large particles and large polydispersity, the ratio between the two averaged quantities is simply equal to the squared modulus of the scattering vector,  $k^2$ , as it can be easily demonstrated in the case of spherical particles. Accordingly, in the condition of large particles, the description provided by Equation 1 still holds and the corresponding value of  $h^*$  is given by a surprisingly simple equation:

$$h^* = \left| \frac{n_m^2 - n_s^2}{n_l^2 - n_s^2} \right| \frac{1}{k} \quad (7)$$

where the modulus of the scattering vector is given by  $k = 4\pi n_s \sin(\theta_s/2)/\lambda$ , and  $\theta_s$  is the angle formed between the scattered and incident ray. For the materials and the set-up geometry employed in this study, in the case of adsorption of SBSAC on the membrane surface,  $h^* = 3.4$  nm. Accordingly, the saturation value at high concentration reported in Figure 2B corresponds to a thickness  $h_{\max}$  of about 2.7 nm. Remarkably, this value is very similar to that obtained with the prism sensor for the same surfactant.

### Comparison of the optical response of reflective and scattering materials

The simplified models developed here enable to evaluate the expected response of different material iso-refractive to water by comparing the values of  $h^*$ , as defined in Equations 2, 5 and 7. As anticipated, the scattering systems can ideally yield higher sensitivity for smaller size of the particles (Equation 5). However, upon increasing the particle size, the parameter  $h^*$  reaches the value for large particles when  $R$  is still significantly smaller than  $\lambda$ . Comparing Equations 5 and 7, in the case of back scattering ( $\theta_s = 180^\circ$ ), the value of  $h^*$  for large spherical particles is reached for  $R = 3\lambda/(4\pi n_s)$ , which, considering the parameters employed in this study, approximately corresponds to values as low as 100 nm.

In order to compare the sensitivity of the prism sensor and the membrane system, a common notation is needed to indicate the direction of the reflected or scattered ray. In the case of the reflective system, the angle of incidence  $\theta_i$  relative to the surface normal can be written in terms of the scattering angle  $\theta_s$  as  $\theta_i = 90^\circ - \theta_s/2$ . Remarkably, the value of  $h^*$  defined in Equation 7 is nearly identical to that of the reflective surface reported in Equation 2, when a common angle  $\theta_s$  is considered. Moreover, the dependence on  $n_l$  is also similar: in both equations  $1/h^*$  roughly scales with  $n_l - n_s$  with a small quadratic correction. Therefore, despite the different optical signal and surface area, the detections based on prism reflectivity and membrane scattering are expected to present a similar dependence on the amount of adsorbing material, at least for membranes with large enough internal structures, as the one considered here (Figure 1B). Indeed, this was experimentally confirmed by the similar saturation values of  $I_R/I_0$  and  $I_S/I_0$  at high amounts of surfactants reported in Figure 2A and 2B, respectively. Moreover, as anticipated, considering the values of  $h^*$ , the obtained thickness  $h_{\max}$  of the adsorbed molecular layer was similar in the two cases, being about 3 nm for both systems.



### III. CHARACTERIZATION OF MOLECULAR ADSORPTION

In the following, we introduce a simple adsorption model, which relates the optical response of the prism and membrane systems to the amount of adsorbing molecules added in solution. Here we consider the equilibrium behavior of adsorption. We show that the response of the membrane is primarily ascribed to the large interfacial area, whereas the adsorption on the prism sensor also depends on the strength of the interaction with the surface.

#### Adsorption model

As shown in Figure 2A and 2B, a saturation of the adsorption signal at high concentration of surfactants was observed for both prism and membrane. However, the saturation intensity  $I_{max}$  was reached at much higher concentrations in the case of the membrane. This difference can be ascribed to the different area of the adsorbing interface, which is much larger in the case of the membrane. This also implies that, at least for the membrane, the dependence of the adsorption signal on the surfactant concentration is dominated by the limited amount of molecules relative to the available adsorption sites. To further investigate this hypothesis, we also performed experiments on SBSAC adsorption increasing the total amount of molecules in solution at fixed concentration. As shown in the insets of Figure 2A and 2B, a signal increase and a saturation were observed also in these experiments, for both the prism and the membrane. This behavior indicates the presence of a large total area available for adsorption with a high affinity for the surfactant, as further discussed in the following.

The theoretical framework for the investigation of the adsorption process was provided by the Langmuir model, arguably the simplest adsorption model, which is based on the assumption of independent binding events onto the surface [39]. Remarkably, this approach was found to well represent the observed behavior despite the possible complexity involving the formation of an adsorbed molecular layer at the solid-liquid interface [23]. The agreement of the extracted value of  $h_{max}$  with the molecular size suggests the formation of a molecular monolayer on the surface. This enabled to model the adsorbing interface as a two-dimensional collection of binding sites and to address the fraction of occupied sites  $\varphi(C_0)$  as a function of the concentration  $C_0$  of molecules added in cuvette. The value of  $\varphi(C_0)$  can be obtained from the thickness  $h$  of the adsorbed layer as  $\varphi(C_0) = h(C_0) / h_{max}$ , which combined with Equation 1 gives

$$\varphi(C_0) = \sqrt{\frac{I(C_0) - I_0}{I_{max} - I_0}} \quad (8)$$

Relevant parameters of the adsorption model are the kinetic constants for adsorption,  $k_{on}$ , and desorption,  $k_{off}$ , as well as their ratio  $K_d = k_{off} / k_{on}$ , which is the equilibrium constant for desorption. Another important parameter is represented by the total amount of binding sites  $N_s$ , which provides the maximum molar quantity of analyte molecules removed from the solution and adsorbed onto the available surface at saturation. In general, large enough values of  $N_s$  are expected to affect both the

equilibrium and the kinetic parameters, since the concentration of analyte in solution may decrease significantly during the adsorption process, yielding mass limitation effects. In this frame, the concentration  $C$  of analyte available in solution is given by

$$C = C_0 - \varphi N_s/V \quad (9)$$

where  $V$  is the volume of the liquid phase and thus the term  $N_s/V$  represents the concentration of adsorption sites in the cuvette and  $\varphi N_s/V$  represents the concentration of molecules adsorbed onto the available surface. Since the adsorption process is substantially governed by the concentration  $C$  of available analytes in solution, according to Equation 9 a similar signal could, in principle, be generated by changing either the concentration  $C_0$  in cuvette or the sample volume  $V$  at some fixed concentration. As anticipated, this behavior was indeed observed for the experimental conditions here employed, as shown in the insets of Figure 2A and 2B. Importantly, the prism set-up enabled to minimize the mass limitation effects through the accessibility of lower values of  $N_s/V$  relative to the membrane system. Nevertheless, the correction of Equation 9 was considered for both materials to properly extract the adsorption parameters. According to the Langmuir model, and considering Equation 9, the progress of  $\varphi$  with time after a change of  $C_0$  or  $V$  is given by

$$\frac{d\varphi(t)}{dt} = k_{on}[C_0 - \frac{N_s}{V}\varphi(t)][1 - \varphi(t)] - k_{off}\varphi(t) \quad (10)$$

In the following we address the equilibrium behavior of Equation 10. The time-dependent behavior will be discussed in Section V for different molecules.

### Equilibrium response of prism and membrane to the amount of adsorbing molecules

Solving Equation 10 for  $d\varphi/dt = 0$  provides the fraction of occupied binding sites at equilibrium,  $\varphi_{eq}$ , for a particular concentration  $C_0$  and for a total amount of molecules  $C_0V$ . The analytical form of  $\varphi_{eq}$  is given by:

$$\varphi_{eq} = \frac{V(C_0+K_d)+N_s - \sqrt{(V(C_0+K_d)+N_s)^2 - 4VC_0N_s}}{2N_s} \quad (11)$$

This equation enables to extract the concentration  $C_{1/2}$  at which half of the binding sites are occupied:

$$C_{1/2} = K_d + \frac{1}{2} \frac{N_s}{V} \quad (12)$$

According to Equation 12, both parameters  $K_d$  and  $N_s$  must be considered in order to account for the experimental behavior of  $\varphi_{eq}(C_0)$  [40]. The values of these parameters were obtained from the concomitant fit of the data of  $\varphi_{eq}$  as a function of  $C_0$  and  $V$  by Equation 11. Figure 2A, 2B and their insets report the curves fitting the data of reflected and scattered intensity, respectively. In the case of the prism sensor, the two sets of data enabled the extraction of both parameters. The  $K_d$  obtained for SBSAC on the prism surface was 165 nM and the corresponding amount of binding sites  $N_s$  was 2.17 nmol. In the case of the membrane, the value of  $K_d$  was assumed to be the same of the prism

and the value of  $N_S$  extracted from the fit was about  $0.88 \mu\text{mol}$ , that corresponds to an available area for adsorption about 400 times larger than that of the prism surface. This value is consistent with the inner surface area obtained from flow resistance measurements performed on commercially available membranes with similar characteristics [41]. Therefore, the membrane system requires larger amount of surfactants to provide the same relative increase of optical signal observed with the prism, because of the larger adsorbing interface. Nevertheless, for applications where the amount of sample is not a relevant limitation, the membrane sensor can still provide practical advantages by enabling a unique combination of filtering and detection capabilities, which can facilitate the development of analytical systems for on-line detection of adsorbing compounds.

#### IV. STRENGTH OF ADSORPTION FOR DIFFERENT MOLECULES

In this section, we compare the behavior of adsorption at equilibrium on the prism sensor for different classes of molecules. We repeat the analysis with the adsorption model introduced in the previous section on different surfactants, a protein and a small hydrophobic molecule. We discuss the thickness of the adsorbing layer and the equilibrium constant for adsorption extracted for the different molecules. We show that the adsorption strength scales with the hydrophobic portion of the molecular contact area on the sensor surface.

##### Equilibrium constant for adsorption

The analysis reported above shows that the planar surface of the prism enables a more comprehensive characterization of the parameters affecting the spontaneous adsorption of molecules relative to the micro-porous membrane. Indeed, according to Equation 12 and as confirmed by the experiments, in the case of the membrane the response to surfactant concentration is ascribed to the large inner surface, whereas, the adsorption on the smaller prism surface depends on the equilibrium constant. Moreover, as it will be discussed in Section V below, the prism also facilitates the kinetic modeling of the molecular transport from the bulk solution onto the surface and vice versa. Therefore, we exploited the prism format to investigate the interaction between different kinds of molecules bearing hydrophobic moieties and the bare surface of the perfluorinated material used to fabricate both the prism and the membrane.

Molecular compounds with refractive index as low as that of water are rare. Therefore, a very large variety of molecules could yield an optical signal upon adsorption on the prism sensor. In order to compare the adsorption of different classes of molecules, we studied three surfactants, the protein lysozyme, and hexane, which is a paraffin that represents an important constituent of gasoline. The chosen surfactants had different net charge and molecular structure. In addition to the cationic surfactant SBSAC, we investigated the anionic sodium dodecyl sulfate (SDS) and the non-ionic polysorbate 20 (Tween 20) (Sigma Aldrich). The physicochemical characteristics of these molecules are reported in Table 1. The experiments were performed either in deionized water (MilliQ®) or using a buffer composition resembling the salinity of a river water (0.049 mM magnesium chloride, 0.09 mM calcium chloride, 1 mM phosphate buffer, 0.27 mM potassium

chloride and 13.7 mM sodium chloride). All the concentrations investigated in this study were well below the expected CMC of the surfactants (Table 1).

Similarly to the study performed on SBSAC, the saturation values of  $h$  extracted about 500 s after the addition of the analyte in cuvette provided a measurement of the equilibrium thickness of the adsorbed layer  $h_{eq}$ , reached for a particular concentration  $C_0$  and for a total amount of molecules  $C_0V$ . Figure 3A and inset report the values of  $h_{eq}(C_0, V)$  for the different molecules considered. By increasing the concentration  $C_0$  or the volume  $V$  at fixed concentration, a saturation of the adsorption was generally observed. Remarkably, the different classes of molecules displayed very different behaviors. The protein lysozyme displayed a response at concentrations much smaller than surfactants, whereas hexane provided a detectable signal at much higher concentrations.

For each molecule, the adsorption curve as a function of  $C_0$  and  $V$  were concomitantly fitted using Equation 11 and the parameters  $K_d$ ,  $N_s$  and  $h_{max}$  were obtained. The results are reported in Table 2. In particular, the obtained  $K_d$  values are in agreement with the typical equilibrium constants reported for similar surfactants adsorbing on solid surfaces [42]. The behaviors of the cationic and non-ionic surfactants were very similar. Surprisingly, also the anionic surfactant in saline buffer presented values of  $K_d$  and  $N_s$  similar to the other surfactants, despite the lower thickness  $h_{max}$  at saturation. These results suggest that the intrinsic affinity of surfactants for the perfluorinated surface does not depend directly on the net-charge of the hydrophilic head, at least in saline buffer. Additionally, the results indicate that, in general, different molecular structures can yield to very similar interaction with the surface. On the other hand, lysozyme and hexane displayed very different affinities and numbers of binding sites on the surface: the values of  $K_d$  and  $N_s$  were order of magnitudes different from those of surfactants. In particular, the protein had a higher affinity (lower value of  $K_d$ ) and fewer binding sites, whereas hexane had a lower affinity and many more adsorption sites. In all cases, it was found that  $N_s/V > K_d$ , hence confirming that the adsorption process was affected by mass limitation.

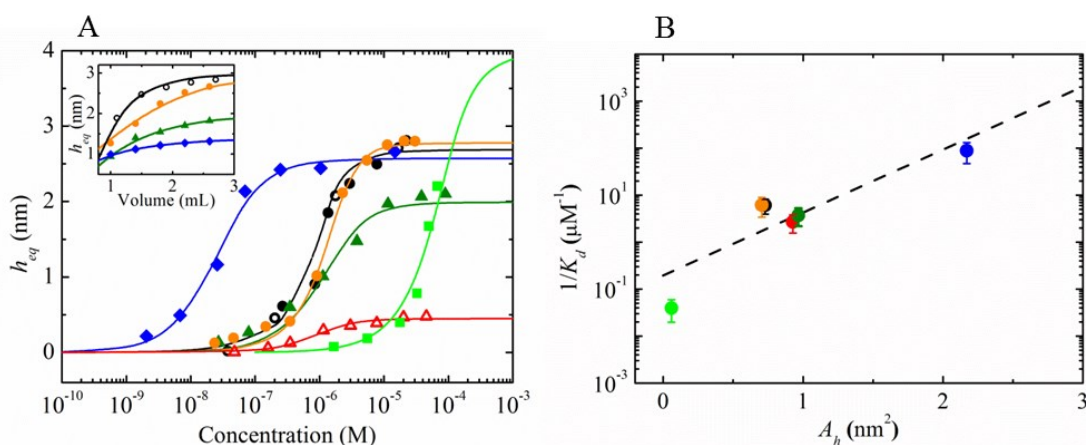


**Figure 3.** Equilibrium of molecular adsorption on the prism surface. The thickness of the adsorbed layer at equilibrium  $h_{eq}$  is reported for different concentrations of SBSAC in deionized water (black open circles) and in saline buffer (orange full circles) and for Tween20 (green full triangles), SDS (red open triangles), lysozyme (blue full diamond) and hexane (light green square) in saline buffer. At each addition, the sample volume in cuvette was increased by 50-200  $\mu\text{L}$ . The lines with corresponding colors represent the fits with Langmuir adsorption model with mass limitation. Inset:  $h_{eq}$  measured as a function of the sample volume at fixed concentration (SBSAC in deionized water: 1.92  $\mu\text{M}$ ; SBSAC in saline buffer: 1.08  $\mu\text{M}$ ; Tween 20: 1.62  $\mu\text{M}$ ; lysozyme: 19.3 nM). The color code is the same as in the main panel.

(B) Value of the equilibrium adsorption constant  $1/K_d$  extracted for each molecule from the fit of the data in panel A as a function of the hydrophobic molecular contact area  $A_h$  on the perfluorinated surface. The color code is the same as in panel A. The black line represents a fit to the data with the function  $\log_{10}(1/K_d) = C_1 + C_2 A_h$ , where  $C_1 = 5.29 (\pm 0.42)$  and  $C_2 = 1.34 (\pm 0.37) \text{ nm}^{-2}$ .

### Thickness of the adsorbed molecular layer

The different molecular classes here investigated showed different increments of reflected intensity at saturation  $I_{max}/I_0$ , as reported in Table 2. Remarkably, similarly to SBSAC, for all the studied surfactants and the protein the corresponding values of  $h_{max}$  were in agreement with the sizes of the molecules (Table 2) [43] estimated by molecular modeling (ChemBioDraw 3D). This indicated the formation of a molecular monolayer at the perfluoropolymer-water interface. For surfactants, the thickness of the adsorption layer also indicated a rather oriented structure of the amphiphilic molecules, which substantially stood on the surface, facing the hydrophobic group toward the plastic material. This interpretation is coherent to other experimental observations of surfactant adsorptions on hydrophobic surfaces made by different techniques for concentrations below the CMC [44][45]. The anionic SDS represented an exception because the value of  $h_{max}$  lower than the molecular size indicated a lower degree of packing relative to the other surfactants. The observed behavior of hexane was different from those of the other molecules: the maximum thickness extrapolated at high concentrations was not compatible with a single molecular layer. In this case, the process could be more rigorously described by a multi-layer adsorption model [46]. Therefore, for hexane the value of  $K_d$  extracted with the Langmuir model represents an upper limit and the thickness of the corresponding monolayer of hexane is derived from the expected geometric packing (Table 2).

### Scaling of the adsorption strength with the molecular contact area

A useful parameter to interpret the different values of adsorption affinities is represented by the contact area per molecule  $A_{mol}$  on the surface. In general, stronger interactions are expected for higher numbers of surface interacting sites per molecule. For instance, it has been observed that larger proteins tend to stick to various kinds of surfaces, whereas smaller ones only adsorb on interfaces with lower wettability [47]. For the studied molecules, the values of  $A_{mol}$  was obtained as  $A_{mol} = V_{mol} / h_{max}$ , where  $V_{mol}$  is the molecular volume estimated either as the molecular mass divided by the density or from the molecular structure. Remarkably, despite the different net charge and geometry, the obtained contact area was similar for all the considered surfactants, being in the range 0.7-1.0  $\text{nm}^2$ . This result is in agreement with the maximum packing obtained from geometrical constraints that was estimated to be in the range 0.8-1.2  $\text{nm}^2$ . As expected, the surface contact areas for lysozyme and hexane were very different from those of surfactants. A value of 7.75  $\text{nm}^2$  was obtained from the adsorption of the protein. This is consistent with the expected packing of the folded molecule onto the surface. Differently, the average contact area per hexane molecule was found to be 0.06  $\text{nm}^2$ , significantly smaller than the estimated geometrical packing of 0.31  $\text{nm}^2$ , in agreement with the hypothesis of the formation of a molecular multi-layer onto the surface, as also derived from the analysis of the thickness of the adsorbed layer.

The experimental observations indicated that the equilibrium constant for adsorption/desorption on the perfluorinated surface does not depend on the net charge of surfactants and depends instead on the class of the molecule (i.e. paraffin vs surfactant vs protein). On the basis of these results, we tested the consistency of a simple model for molecular adsorption on the perfluorinated surface. We assumed that only the hydrophobic moieties of the molecules adhere to the surface and that all the hydrophobic interactions have the same strength per unit surface. With these assumptions, a linear scaling of the binding free energy with the hydrophobic portion  $A_h$  of the molecular contact area  $A_{mol}$  is expected. In the case of hexane and all the surfactants, the measured contact area  $A_{mol}$  was all ascribed to hydrophobic moieties, therefore  $A_h = A_{mol}$ . Differently, only a fraction of the amino acids composing the protein lysozyme could be considered hydrophobic. Accordingly, in this case we assumed  $A_h = f_h \cdot A_{mol}$ , where  $f_h = 0.28$  was obtained as the fraction of hydrophobic residues (W, F, Y, L, I, C, M) over the entire protein sequence [48]. Figure 3B reports the measured value of the equilibrium constant for adsorption  $1/K_d$  as a function of  $A_h$ . Remarkably, despite the diversity of the molecules, a scaling of  $\log(1/K_d)$  with  $A_h$  was observed. From this dependence, we derived a free energy increment for molecular adsorption of about  $-1.83 \text{ kcal mol}^{-1} \text{ nm}^{-2}$ . This value is in agreement with the adsorption free energy per hydrocarbon unit reported in previous works, which typically is in the range  $0.2\text{-}0.6 \text{ kcal mol}^{-1}$ [49][50][42]. Moreover, the estimated adsorption strength is coherent with the reported free energy of hydrophobic interactions among amino acids [51]. Overall, these observations are in agreement with the hypothesis of a relevant contribution of the hydrophobic contact area to the adsorption free energy on the perfluorinated surface and suggest the validity of this approach to predict the surface binding affinity from the molecular size and structure.

## V. KINETICS OF TRANSPORT AND ADSORPTION

In this section, we report the measured adsorption kinetics for the different molecular compounds addressed in the previous section. We analyze the data using the time-dependent Langmuir model for adsorption introduced in section III, which accounts for mass limitation effects. Additionally, we consider the effect of transport limitation on the observed kinetics and propose a suitable model, which relates the adsorption kinetics to a transport parameter that ultimately depends on the molecular size.

### Observed adsorption kinetics

The label-free detection based on the prism set-up also enabled direct access to the adsorption kinetics. The adsorption formula reported in Equation 10 provides the time behavior of  $\varphi(t)$ . The general analytic form of  $\varphi(t)$  is a hyperbolic tangent, which, in practice, differs only slightly from a single exponential behavior for all the conditions of interest in this study. This is because the coefficient of the term linear in  $\varphi$  is always larger than that of the quadratic one. Therefore, fitting the experimental adsorption curves with single exponential functions practically represents a good approximation and provides a robust approach to extract the kinetics parameter of the process.

Figure 4A reports the thickness increment  $\Delta h(t) = h(t) - h(0)$  measured on the prism after a change of SBSAC concentration in cuvette at  $t = 0$ . The adsorption of SBSAC reached an

equilibrium within a few minutes after the addition of surfactant. The observed kinetics became faster at higher concentrations. The growth  $\Delta h$  was well fitted by single exponential curves, as expected. Notably, also the adsorption curves measured after a change of volume were well fitted by single exponential functions, as shown in Figure 4B.

We extracted the characteristic rate for adsorption  $\Gamma(C_0, V)$  for the different molecular compounds considered in Section IV. The rates measured as a function of the concentration  $C_0$  are plotted in Figure 5A. Generally, the rate increased with the concentration of analyte, in agreement with the Langmuir model of Equation 10. The data points can be grouped in three classes corresponding to the three kinds of molecules. All surfactants had rather similar kinetics, coherently with the results obtained from the equilibrium analysis. The protein also showed a behavior at low concentrations similar to that of surfactants, whereas the kinetics at high concentrations became much faster. On the contrary, the hexane data indicated a much slower adsorption kinetics. In general, the observed rates were in agreement with other studies on the kinetic of surfactant adsorption performed below the CMC [45][52]. The inset of Figure 5A reports the rates as a function of the sample volume in cuvette at constant concentration. In agreement with Equation 10, the observed decrease of  $\Gamma(V)$  was ascribed to the effect of mass limitation, as further discussed below.

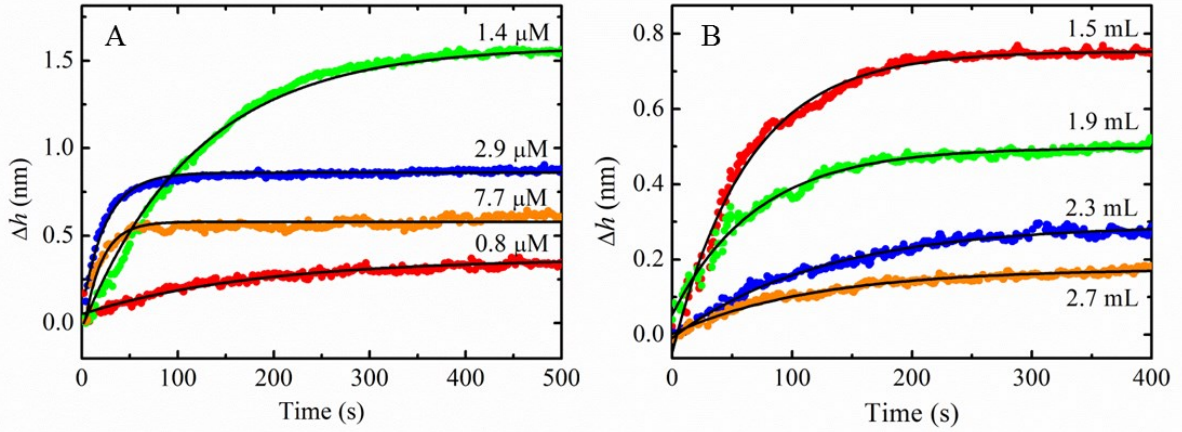


**Figure 4.** Adsorption curves measured with the prism sensor. (A) Increment of the adsorbed layer thickness  $\Delta h$  as a function of time after the addition of increasing concentrations of SBSAC in deionized water. The black lines represent exponential fitting curves. (B) Adsorption curves  $\Delta h$  of SBSAC in deionized water and exponential fits (black lines) obtained for increasing sample volumes at fixed concentration  $C_0 = 1.92 \mu\text{M}$ .

### Kinetic model for adsorption

In order to compare the measured adsorption rates with those predicted by the model, we calculated effective adsorption rates from Equation 10. We considered the initial, linear growth of adsorption after a concentration or volume increase. In the case of an exponential growth with amplitude  $\varphi_{eq}$  and rate  $\Gamma$ , the initial slope is given by the product  $\varphi_{eq}\Gamma$ . On the other hand, according to Equation 10, the initial slope of  $\varphi(t)$  is always equal to  $k_{on}C_0$ . Accordingly, we modeled the rate of adsorption as

$$\Gamma = \frac{k_{on}C_0}{\varphi_{eq}} \quad (13)$$

where  $\varphi_{eq}$  is given by Equation 11. In the case of negligible mass limitation, that is for  $N_s/V \ll K_d$ , the rates are described by the simple analytical form  $\Gamma = k_{on}C_0 + k_{off}$ . More generally, the expression of  $\Gamma$  becomes simple for very small and very large values of the analyte concentration  $C_0$  relatively to  $C_{1/2}$ , and for  $C_0 = C_{1/2}$ . In these limits,  $\Gamma = k_{on}(N_s/V) + k_{off}$ ,  $\Gamma = k_{on}C_0$ , and  $\Gamma = k_{on}(N_s/V) + 2k_{off}$ , respectively. Therefore, the mass limitation effect tends to increase the observed rate through the term  $k_{on}(N_s/V)$ . Importantly, for sufficiently large analyte concentrations, the adsorption rate is always given by  $k_{on}C_0$ , and, therefore, it is not affected by mass limitation. This allowed to directly extract the apparent kinetic constant for adsorption  $k_{on}$  from the slope of the rate  $\Gamma(C_0)$  measured for the largest concentrations.

In practice, the data reported in Figure 5A were fitted using Equation 13, constraining the values of  $N_s$  and  $K_d = k_{off}/k_{on}$  to those previously extracted from the study of the equilibrium data (Table 2). In this way, only one free parameter (either  $k_{on}$  or  $k_{off}$ ) was determined by the fit. The obtained fitting curves are reported in Figure 5A and inset, and the values of  $k_{on}$  and  $k_{off}$  are reported in Table 2. As expected from the visual inspection of the behavior of  $\Gamma(C_0)$ , the desorption kinetic constant  $k_{off}$  was rather similar for the three surfactants and the protein, whereas the kinetic constant for adsorption was larger for the protein. Both kinetic constants extrapolated for hexane were much lower than those of the other molecules.

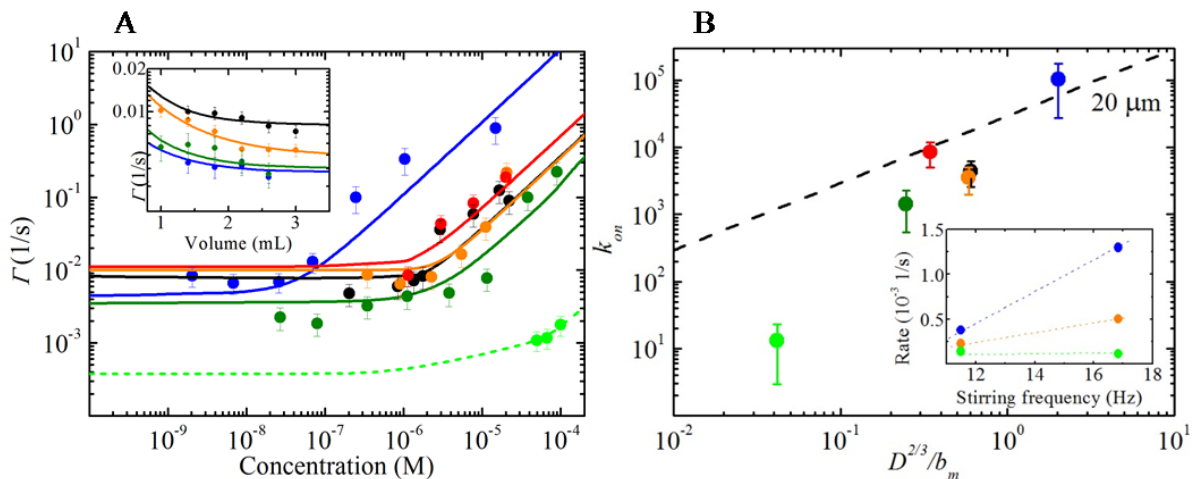


**Figure 5.** Kinetics of molecular adsorption on the perfluorinated surface. The rates  $\Gamma$  extracted from the exponential fit of the adsorption curves are reported as a function of the concentration of SBSAC in deionized water (black open circles) and in saline buffer (orange full circles) and for Tween20 (green full triangles), SDS (red open triangles), lysozyme (blue full diamond) and hexane (light green square) in saline buffer. The lines with corresponding color represent linear fits. Inset:  $\Gamma$  measured as a function of the sample volume at fixed concentration (SBSAC in deionized water: 1.92  $\mu\text{M}$ ; SBSAC in saline buffer: 1.08  $\mu\text{M}$ ; Tween 20: 1.62  $\mu\text{M}$ ; lysozyme: 19.3 nM). The color code is the same as in the main panel. (B) Value of the observed kinetic constant for adsorption  $k_{on}$  as a function of  $D^{2/3}/b_m$ . The dashed line represents the expected behavior for a constant depletion layer of 20  $\mu\text{m}$ . Inset: dependence of the measured adsorption rate on the stirring velocity at fixed concentration of SBSAC in saline buffer (orange,  $C_0 = 3.3 \mu\text{M}$ ), lysozyme (blue,  $C_0 = 71 \text{ nM}$ ) and hexane (light green,  $C_0 = 55.6 \mu\text{M}$ ).

### Effect of transport limitation

In analogy to the case of ligand-receptor binding, the observed adsorption and desorption process could be affected by the limited transport of analyte molecules from the bulk solution to the sensing surface. This condition occurs when the mixing of molecules in the proximity of the surface is not



fast enough in comparison to the intrinsic kinetics for molecular binding, hence leading to smaller values of the measured kinetic rates. An extensive description of transport limitation phenomena in surface binding processes is provided in [53]. Processes characterized by faster binding kinetics in general are more affected by such transport limitation effect. Importantly, the adsorption kinetics measured in this study were much faster than those typically observed for specific antibody-antigen binding performed with a similar measuring system [10]. Additionally, in the case of adsorption, the transport contribution may play a non-negligible role even for very high flow rates, because of the high densities of binding sites on the surface [53]. This is, in fact, an inevitable condition for non-specific adsorption processes. In the experimental set-up employed here, the use of a magnetic stirring bar provided the advantage of a rather efficient mixing of a relatively large volume of solution, approaching the turbulent regime at the highest stirring rates. Nevertheless, extremely large, and substantially impractical flow rates or stirring speeds may be required to reduce the effect of transport limitations in the case of large densities of surface binding sites. Therefore, transport phenomena were expected to play a role in the observed adsorption kinetics. Indeed, an indication of the relevance of the transport limitation was given by the dependence of the observed adsorption kinetics on the stirring speed. As shown in the inset of Figure 5B, the measured adsorption rates of hexane was almost insensitive to the rotational speed of the stirrer, whereas those of SBSAC surfactant and lysozyme strongly depended on it. This indicated a more relevant contribution of transport limitation for the surfactants and the protein.

### Dependence of the observed adsorption kinetics on the molecular size

In the case of kinetics affected by transport limitation, a rather thick layer of fluid in contact with the adsorbing interface experiences a lower concentration of analyte relative to the bulk solution. In this condition, the measured rate is limited by the diffusion time across such depletion layer. Accordingly, the value of the measured kinetic constants  $k_{on}$  and  $k_{off}$  are lower than those of the intrinsic kinetic constants  $k_{on}^i$  and  $k_{off}^i$ , which depend only on the interactions between the analyte molecules and the surface. In particular, considering the effects of transport due to the sample flow and diffusion across the depletion layer, it can be demonstrated (see Appendix B) that the apparent rate  $k_{on}$  observed for  $C_0 \gg C_{1/2}$  must be in the range  $k_{on}^{tl} < k_{on} < k_{on}^i$ , where the transport-limited rate  $k_{on}^{tl}$  is given by

$$k_{on}^{tl} = F \frac{D^{\frac{2}{3}}}{b_m} \quad (14)$$

and  $D$  and  $b_m$  are the diffusion coefficient of the molecule and the surface density of adsorption sites, respectively. The parameter  $F$  contains all the terms that depend on the cell geometry and flow, and not on the properties of the adsorbing molecule. Its value is given by  $F = (\dot{\gamma}/L)^{1/3}$ , where  $L$  is the length of the adsorption area of the sensor along the flow direction and  $\dot{\gamma}$  is the derivative of the flux along the surface normal. Similar equations for the transport-limited rate are often encountered in studies concerning sensors in micro-fluidic cell formats [54][55]. Here we extend the model to the cuvette-based cell and focus on the parameters  $D$  and  $b_m$  that depend on the specific adsorbing molecule. Figure 5B reports the measured values of  $k_{on}$  as a function of  $D^{2/3}/b_m$ . The dashed line indicates the expected scaling for a fully transport-limited case, assuming a

thickness  $\delta$  of the depletion layer of 20  $\mu\text{m}$ . This represents an upper limit for the value of  $\delta$  obtained assuming that  $k_{on} = k_{on}^{tl}$  and that  $b_m$  equals the reciprocal of the molecular contact area onto the surface,  $1/A_{\text{mol}}$ . In practice, this is the largest value of  $\delta$  in agreement with the measured values of  $k_{on}$  for all the surfactants and the lysozyme. Indeed, Figure 5B shows that the kinetic rates for adsorption measured for the surfactants and the protein were consistent with the dependence indicated in Equation 14, whereas hexane did not follow the same scaling. Consequently, the measured kinetics of the surfactants and the protein were consistent with a fully transport-limited regime. Differently, the slower adsorption rates of hexane indicated that transport was not the limiting process in this case, and the observed  $k_{on}$  can be ascribed to the molecule-surface interaction.

Remarkably, the scaling indicated by Equation 14 provided a tool to quantitatively discriminate among the adsorption kinetics of different molecules. In fact, both terms  $D$  and  $b_m$  scales with the size of the analyte, either through its hydrodynamic radius or the contact area onto the sensing surface, respectively. As reported above, the strength of the adsorption interaction at equilibrium was found to scale with the hydrophobic contact area of the molecule. Here we linked the observed transport-limited kinetics to other parameters derived from the molecular size. Overall, the analysis of the adsorption kinetics, in combination with that on the equilibrium discussed in section IV, indicated that the measurement of the spontaneous adsorption on the Hyflon® AD surfaces enables to detect the presence of different classes of molecules in solution and to discriminate them on the basis of their size and hydrophobicity.

## VI. CONCLUSIONS

The work presented here provides a threefold advancement in the development of novel label-free, optical detection systems based on fluorinated materials index-matched with water: (i) We demonstrated the production of a new class of perfluorinated materials in the form of micro-porous membrane; (ii) We developed an analytical model to account for the optical response upon adsorption of different index-matched materials finding a surprisingly simple similarity between the sensitivity of the reflectance- and scattering-based systems; (iii) By means of experimental characterization and modeling of the adsorption of different molecular compounds on a planar surface, we identified main molecular features affecting the selectivity of the adsorption process.

Remarkably, the adsorption behaviors for different surfactants, a protein and an oil were very different. In contrast, all the studied surfactants displayed a similar behavior, despite the different net charge and structure. The molecular size and the molecular area in contact with the surface upon adsorption were identified as relevant parameters, through different specific mechanisms:

- the optical response scaled with the squared molecular size affecting the thickness of the adsorption layer;
- the strength of the adsorption interaction at equilibrium was found to scale with the molecular hydrophobic contact area on the perfluorinated surface;
- for the fastest adsorption kinetics, where the transport phenomena became the limiting effect, the observed adsorption rate scaled with the molecular contact area times  $D^{2/3}$ , where, in general, the diffusion coefficient  $D$  scales with the reciprocal molecular size.

These results indicate that, if properly controlled and tuned, the spontaneous adsorption on perfluorinated materials index-matched with water enables the selective detection of different molecular compounds. The selectivity is achieved considering the amplitudes and kinetics of the optical response, possibly at different dilutions. Accordingly, even molecular classes with similar refractive index, as in the case of proteins and surfactants, can be identified through the analysis of the adsorption curves. This provides the basis to design a new class of optical sensors combining sensitivity, robustness, reusability and reduced instrumental complexity. These features are constantly sought for different applications and, in particular, for deployable, on line detection systems for environmental monitoring. As an example, a water basin could be autonomously screened using the optical detection method here presented, and when the response is above a pre-defined threshold, suitable amounts of sample can be collected and stored for more specific, lab-based analysis. In this way, the label-free detection based on fluorinated plastics can effectively complement and improve the current analytical approaches for continuous environmental monitoring.

## **ACKNOWLEDGMENTS**

This work was supported by EU (NAPES Project – NMP-2013-SMALL-7, project no. 604241).

## APPENDIX A. PRODUCTION OF MICRO-POROUS MEMBRANES

The membranes of Hyflon® AD40 (Solvay Specialty Polymers, Italy) were realized by Non-Solvent Induced Phase Separation method [56]. We dissolved 7.5 g of the perfluorinated polymer into 30 mL of methoxyperfluorobutane, HFE 7100 (3M-Novec) and 2.5 g of cyclohexanone (Sigma-Aldrich). This solution was used to realize a 250  $\mu\text{m}$  film by casting on a glass plate cooled with dry ice. The plate was then immediately placed into a coagulation bath composed by a 1:1 mixture of acetone and ethanol for 10 minutes. Then, the plate was immersed in a bath of ethanol for others 10 minutes to extract the residual solvent. We stored the samples in a 30%-70% mixture of ethanol and water. We obtained membranes with a thickness of 80-100  $\mu\text{m}$  and porosity of 60%-70%. The thermo-gravimetric analysis revealed only 1% wt of residual solvent in the membranes. The cross-section SEM image (Figure1.B) was taken after breaking the sample in liquid nitrogen, without any kind of metallization. Before the optical measurements, we washed the membrane with MilliQ water several times and then we soaked it for 15 hours with water. Finally, we degassed the sample for 10 minutes to remove the air bubbles.

The refractive index of the membrane was obtained as the extrapolated minimum of scattered light as a function of the refractive index of the solvent. The membranes were soaked in different mixtures of water and ethanol, whose refractive index were measured by an Abbe refractometer. The measurements gave a membrane refractive index of  $n = 1.3309 \pm 0.0002$ .

## APPENDIX B. TRANSPORT-LIMITED ADSORPTION KINETICS

In general, binding or adsorption processes are characterized by intrinsic kinetic constants  $k_{on}^i$  and  $k_{off}^i$  that depend on the interactions between the analyte molecules and the surface. Only in the case of fast enough transport of molecules (i.e., fast flow and mixing near the surface),  $k_{on}^i$  and  $k_{off}^i$  are equal to the observed kinetic constants  $k_{on}$  and  $k_{off}$ , respectively. More generally, the transport process may somewhat affect both the observed kinetic constants  $k_{on}$  and  $k_{off}$  in the same way. The condition of transport limitation involves the presence of a layer of fluid on the surface with a transiently lower concentration of analyte relative to the bulk solution. The measured rate is affected by the diffusion across such depletion layer. The thickness  $\delta$  of the depletion zone depends on the flux close to the surface, on the geometry of the measuring cell and on the free diffusion of the studied molecule. The value of  $\delta$  can be estimated as [53]:

$$\delta = \sqrt[3]{\frac{LD}{\dot{\gamma}}} \quad (15)$$

where  $L$  is the length of the adsorption area of the sensor along the flow direction,  $\dot{\gamma}$  is the derivative of the flux along the surface normal and  $D$  is the diffusion coefficient of the molecule. In general, transport limitation is more relevant for larger values of  $\delta$ . However, according to Equation 15,  $\delta$  scales only with the cube root of the flow parameter  $\dot{\gamma}$ .

A common approach to compute the effect of transport on the observable kinetic rates is to consider two regions (i.e., two compartments) with different concentrations of analyte: the depletion layer and the rest of the sample volume. The two compartments have two spatially uniform concentrations,  $C_d(t)$  and  $C_{bulk}(t)$ , respectively [57]. Using this approximation, the adsorption

process was still modeled by Equation 10 with the substitution  $C_0 = C_d$ , and with the value of  $C_d$  provided by the diffusive equilibrium between the two compartments. Considering an initial condition without analyte molecules in cuvette and a sudden increase of concentration from zero to  $C_{bulk}$ , for a negligible value of  $\delta$  the initial flux of molecules toward the surface is given by  $J^{kin} = k_{on}^i C_{bulk} b_m$ , where  $b_m$  represents the surface density of available binding sites. At the other extreme, a purely diffusive flux across the depletion layer is given by  $J^{diff} = D C_{bulk} / \delta$ , according to Fick's first law of diffusion. The ratio  $Da = J^{kin} / J^{diff}$  is known as the Damköhler number and its value indicates to what extent the observed kinetics is affected by transport limitation [53][54]. The measured characteristic time  $\tau_{obs} = 1/\Gamma$  for a binding process on a surface differs from the intrinsic molecular interaction time  $\tau_R = (k_{on}^i C_0 + k_{off}^i)^{-1}$  according to:

$$\tau_{obs} = (1 + Da)\tau_R \quad (16)$$

In the case of pronounced transport limitation ( $Da \gg 1$ ) and for  $C_0 \gg C_{1/2}$ , from the above definition of  $Da$  we derived that  $\Gamma = k_{on}^{tl} C_0$ , where

$$k_{on}^{tl} = \frac{D}{\delta b_m} \quad (17)$$

represents the transport-limited rate for adsorption. Accordingly, the value of the apparent kinetic constant for binding  $k_{on}$  must be in the range  $k_{on}^{tl} < k_{on} < k_{on}^i$ .

In order to investigate the dependence of the observed adsorption kinetics on the molecular properties, we focused on the limiting case of a fully transport-limited process. Substituting the expression of  $\delta$  given in Eq. 15 into Eq. 17, the terms that depend on the cell geometry and flow and not on the properties of the molecular analyte were grouped in the parameter  $F = (\dot{\gamma}/L)^{1/3}$ , thus leading to Equation 14.

## References

- [1] B. Zhmud, F. Tiberg, Interfacial dynamics and structure of surfactant layers, *Adv. Colloid Interface Sci.* **113**, 21–42 (2005).
- [2] F. Zaera, Probing liquid/solid interfaces at the molecular level, *Chem. Rev.* **112**, 2920–2986 (2012).
- [3] B. Stuart, Infrared Spectroscopy, in: *Kirk-Othmer Encycl. Chem. Technol.*, John Wiley & Sons, Inc., Hoboken, NJ, USA, (2005).
- [4] P. Patnaik, *Handbook of Environmental Analysis: Chemical Pollutants in Air, Water, Soil, and Solid Wastes*, Second Edition, (2010).
- [5] S. González, D. Barceló, M. Petrovic, Advanced liquid chromatography-mass spectrometry (LC-MS) methods applied to wastewater removal and the fate of surfactants in the environment, *TrAC - Trends Anal. Chem.* **26**, 116–124 (2007).
- [6] T. Reemtsma, Liquid chromatography-mass spectrometry and strategies for trace-level analysis of polar organic pollutants, *J. Chromatogr. A.* **1000**, 477–501 (2003).
- [7] M. Shim, N.W.S. Kam, R.J. Chen, Y. Li, H. Dai, Functionalization of Carbon Nanotubes for Biocompatibility and Biomolecular Recognition, *Nano Lett.* **2**, 285–288 (2002).
- [8] S. Wu, Q. He, C. Tan, Y. Wang, H. Zhang, Graphene-based electrochemical sensors, *Small.* **9**, 1160–1172 (2013).
- [9] B.R. Baker, R.Y. Lai, M.S. Wood, E.H. Doctor, A.J. Heeger, K.W. Plaxco, An electronic, aptamer-based small-molecule sensor for the rapid, label-free detection of cocaine in adulterated samples and biological fluids, *J. Am. Chem. Soc.* **128**, 3138–3139 (2006).
- [10] F. Giavazzi, M. Salina, R. Cerbino, M. Bassi, D. Prosperi, E. Ceccarello, et al., Multispot, label-free biodetection at a phantom plastic-water interface., *Proc. Natl. Acad. Sci. U. S. A.* **110**, 9350–5 (2013).
- [11] F. Giavazzi, M. Salina, E. Ceccarello, A. Ilacqua, F. Damin, L. Sola, et al., A fast and simple label-free immunoassay based on a smartphone, *Biosens. Bioelectron.* **58**, 395–402 (2014).
- [12] R. Lanfranco, M. Buscaglia, Invisible Fluorinated Materials for Optical Sensing, in: *Ref. Modul. Mater. Sci. Mater. Eng.*, Elsevier, (2016).
- [13] D. Prosperi, C. Morasso, F. Mantegazza, M. Buscaglia, L. Hough, T. Bellini, Phantom nanoparticles as probes of biomolecular interactions., *Small.* **2**, 1060–7 (2006).
- [14] C. Morasso, M. Colombo, S. Ronchi, L. Polito, S. Mazzucchelli, D. Monti, et al., Towards a universal method for the stable and clean functionalization of inert perfluoropolymer nanoparticles: Exploiting photopolymerizable amphiphilic diacetylenes, *Adv. Funct. Mater.* **20**, 3932–3940 (2010).
- [15] A. Ghetta, D. Prosperi, F. Mantegazza, L. Panza, S. Riva, T. Bellini, Light scattered by model phantom bacteria reveals molecular interactions at their surface., *Proc. Natl. Acad. Sci. U. S. A.* **102**, 15866–70 (2005).
- [16] M. Salina, F. Giavazzi, E. Ceccarello, F. Damin, M. Chiari, M. Ciuffo, et al., Multi-spot, label-free detection of viral infection in complex media by a non-reflecting surface, *Sensors Actuators B Chem.* **223**, 957–962 (2016).
- [17] W.H. Tuminello, Solubility of Poly(Tetrafluoroethylene) and its Copolymers, in:

Fluoropolymers 2, Kluwer Academic Publishers, Boston, n.d.: pp. 137–143.

- [18] B. Jones, Fluoropolymers for Coating applications, *JCT Coatingstech.* **5**, 44–48 (2008).
- [19] E. Giannetti, Semi-crystalline fluorinated polymers, *Polym. Int.* **50**, 10–26 (2001).
- [20] T. Bellini, V. Degiorgio, F. Mantegazza, F.A. Marsan, C. Scarnecchia, Electrokinetic properties of colloids of variable charge. I. Electrophoretic and electro-optic characterization, *J. Chem. Phys.* **103**, 8228 (1995).
- [21] F. Mantegazza, T. Bellini, M. Buscaglia, V. Degiorgio, D.A. Saville, Electrokinetic properties of colloids of variable charge. III. Observation of a Maxwell–Wagner relaxation mechanism by high-frequency electric-birefringence spectroscopy, *J. Chem. Phys.* **113**, 6984 (2000).
- [22] M. Rabe, D. Verdes, S. Seeger, Understanding protein adsorption phenomena at solid surfaces, *Adv. Colloid Interface Sci.* **162**, 87–106 (2011).
- [23] R. Atkin, V.S.J. Craig, E.J. Wanless, S. Biggs, Mechanism of cationic surfactant adsorption at the solid-aqueous interface, *Adv. Colloid Interface Sci.* **103**, 219–304 (2003).
- [24] J.L. Wolgemuth, R.K. Workman, S. Manne, Surfactant aggregates at a flat, isotropic hydrophobic surface, *Langmuir.* **16**, 3077–3081 (2000).
- [25] S. Paria, K.C. Khilar, A review on experimental studies of surfactant adsorption at the hydrophilic solid-water interface, *Adv. Colloid Interface Sci.* **110**, 75–95 (2004).
- [26] S.O. Nielsen, G. Srinivas, C.F. Lopez, M.L. Klein, Modeling Surfactant Adsorption on Hydrophobic Surfaces, *Phys. Rev. Lett.* **94**, 228301 (2005).
- [27] X. López-Lozano, L.A. Pérez, I.L. Garzón, Enantiospecific Adsorption of Chiral Molecules on Chiral Gold Clusters, *Phys. Rev. Lett.* **97**, 233401 (2006).
- [28] C. Brumaru, M.L. Geng, Interaction of surfactants with hydrophobic surfaces in nanopores, *Langmuir.* **26**, 19091–19099 (2010).
- [29] E. Finot, A. Fabre, A. Passian, T. Thundat, Dynamic and Static Manifestation of Molecular Absorption in Thin Films Probed by a Microcantilever, *Phys. Rev. Appl.* **1**, 024001 (2014).
- [30] D. Lohse, X. Zhang, Surface nanobubbles and nanodroplets, *Rev. Mod. Phys.* **87**, 981–1035 (2015).
- [31] C. Toccafondi, M. Prato, G. Maidecchi, A. Penco, F. Bisio, O. Cavalleri, et al., Optical properties of Yeast Cytochrome c monolayer on gold: An in situ spectroscopic ellipsometry investigation, *J. Colloid Interface Sci.* **364**, 125–132 (2011).
- [32] I. Solano, P. Parisse, F. Gramazio, O. Cavalleri, G. Bracco, M. Castronovo, et al., Spectroscopic ellipsometry meets AFM nanolithography: about hydration of bio-inert oligo(ethylene glycol)-terminated self assembled monolayers on gold, *Phys. Chem. Chem. Phys.* **17**, 28774–28781 (2015).
- [33] F.L. Pedrotti, L.M. Pedrotti, L.S. Pedrotti, *Introduction To Optics*, 3/E, 3rd Editio, Addison-Wesley, (2006).
- [34] V. Arcella, A. Ghielmi, G. Tommasi, High Performance Perfluoropolymer Films and Membranes, *Ann. N. Y. Acad. Sci.* **984**, 226–244 (2003).
- [35] P. Wiltzius, F.S. Bates, S.B. Dierker, G.D. Wignall, Structure of porous vycor glass, *Phys. Rev. A.* **36**, 2991–2994 (1987).

- [36] L. Cipelletti, M. Carpineti, M. Giglio, Fractal Morphology, Spatial Order, and Pore Structure in Microporous Membrane Filters, *Langmuir*. **12**, 6446–6451 (1996).
- [37] H.C. van de Hulst, *Light Scattering by Small Particles*, Dover, New York, (1957).
- [38] R. Piazza, V. Degiorgio, Light scattering study of spherical latex particles: Measurement of surfactant adsorption and of intrinsic anisotropy, *Opt. Commun.* **92**, 45–49 (1992).
- [39] P. Atkins, J. de Paula, *Atkins' Physical Chemistry*, 9th ed., OUP Oxford, (2010).
- [40] B. Esteban Fernández de Ávila, H.M. Watkins, J.M. Pingarrón, K.W. Plaxco, G. Palleschi, F. Ricci, Determinants of the Detection Limit and Specificity of Surface-Based Biosensors, *Anal. Chem.* **85**, 6593–6597 (2013).
- [41] E. Iritani, S. Tachi, T. Murase, Influence of protein adsorption on flow resistance of microfiltration membrane, *Colloids Surfaces A Physicochem. Eng. Asp.* **89**, 15–22 (1994).
- [42] J.T.K. Milton J. Rosen, *Surfactants and Interfacial Phenomena*, 4th ed., Wiley, (2012).
- [43] N.G. Gaylord, J.H. Gibbs, *Physical chemistry of macromolecules. C. TANFORD*. Wiley, New York, *J. Polym. Sci.* **62** (1962).
- [44] S.F. Turner, S.M. Clarke, a. R. Rennie, P.N. Thirtle, D.J. Cooke, Z.X. Li, et al., Adsorption of Sodium Dodecyl Sulfate to a Polystyrene/Water Interface Studied by Neutron Reflection and Attenuated Total Reflection Infrared Spectroscopy, *Langmuir*. **15**, 1017–1023 (1999).
- [45] R. Atkin, V.S.J. Craig, S. Biggs, Adsorption kinetics and structural arrangements of cationic surfactants on silica surfaces, *Langmuir*. **16**, 9374–9380 (2000).
- [46] A.J. Ricco, G.C. Frye, S.J. Martin, Determination of BET surface areas of porous thin films using surface acoustic wave devices, *Langmuir*. **5**, 273–276 (1989).
- [47] G.B. Sigal, M. Mrksich, G.M. Whitesides, Effect of surface wettability on the adsorption of proteins and detergents, *J. Am. Chem. Soc.* **120**, 3464–3473 (1998).
- [48] W.C. Wimley, S.H. White, Experimentally determined hydrophobicity scale for proteins at membrane interfaces, *Nat. Struct. Biol.* **3**, 842–848 (1996).
- [49] K.D. Danov, P.A. Kralchevsky, The standard free energy of surfactant adsorption at air/water and oil/water interfaces: Theoretical vs. empirical approaches, *Colloid J.* **74** (2012) 172–185.
- [50] S.H. Chen, C.W. Frank, Infrared and fluorescence spectroscopic studies of self-assembled n-alkanoic acid monolayers, *Langmuir*. **5**, 978–987 (1989).
- [51] W.C. Wimley, S.H. White, Experimentally determined hydrophobicity scale for proteins at membrane interfaces, *Nat. Struct. Biol.* **3**, 842–848 (1996).
- [52] A.A. Levchenko, B.P. Argo, R. Vidu, R. V. Talroze, P. Stroeve, Kinetics of sodium dodecyl sulfate adsorption on and desorption from self-assembled monolayers measured by surface plasmon resonance, *Langmuir*. **18**, 8464–8471 (2002).
- [53] T.M. Squires, R.J. Messinger, S.R. Manalis, Making it stick: convection, reaction and diffusion in surface-based biosensors., *Nat. Biotechnol.* **26**, 417–26 (2008).
- [54] R. Hansen, H. Bruus, T.H. Callisen, O. Hassager, Transient convection, diffusion, and adsorption in surface-based biosensors, *Langmuir*. **28**, 7557–7563 (2012).
- [55] P. Schuck, Kinetics of ligand binding to receptor immobilized in a polymer matrix, as detected with an evanescent wave biosensor. I. A computer simulation of the influence of mass transport., *Biophys. J.* **70**, 1230–1249 (1996).



- [56] R.W. Baker, *Membrane Technology and Applications*, 3rd ed., Wiley, (2012).
- [57] D.G. Myszka, X. He, M. Dembo, T.A. Morton, B. Goldstein, Extending the range of rate constants available from BIACORE: interpreting mass transport-influenced binding data., *Biophys. J.* **75**, 583–594 (1998).
- [58] J. Vörös, The density and refractive index of adsorbing protein layers., *Biophys. J.* **87**, 553–561 (2004).
- [59] R.M. Weinheimer, D.F. Evans, E. Cussler, Diffusion in surfactant solutions, *J. Colloid Interface Sci.* **80**, 357–368 (1981).
- [60] H. Gao, R. Zhu, X. Yang, S. Mao, S. Zhao, J. Yu, et al., Properties of polyethylene glycol (23) lauryl ether with cetyltrimethylammonium bromide in mixed aqueous solutions studied by self-diffusion coefficient NMR, *J. Colloid Interface Sci.* **273**, 626–631 (2004).
- [61] D. Brune, S. Kim, Predicting protein diffusion coefficients., *Proc. Natl. Acad. Sci.* **90**, 3835–3839 (1993).
- [62] C.R. Wilke, P. Chang, Correlation of diffusion coefficients in dilute solutions, *AIChE J.* **1**, 264–270 (1955).

**Table 1. Physical parameters of the studied molecules.**

Molecule	MW <sup>1</sup> (Da)	CMC <sup>2</sup> (mM)	$\rho^1$ (g/mL)	$n^3$	$D^3$ (10 <sup>-6</sup> cm <sup>2</sup> /s)	$h^*$ (nm)
SBSAC deion. water	442.15	0.34	0.376	1.435	4	3.2
SBSAC buffer		0.13				
Tween 20	1227.54	0.30	1.1	1.469	1	2.4
SDS	288.37	0.54	1.01	1.461	1.76	2.5
Lysozyme	14000		1.2	1.5	1.10	1.9
Hexane	86.18		0.655	1.373	2.3	8.4

<sup>1</sup>Molecular mass and density were taken from the data sheets of the compounds or from [58] in the case of Lysozyme.

<sup>2</sup>CMC was obtained by electrical conductivity measurements. <sup>3</sup>Refractive indices and diffusion coefficients were taken from references [59][60][61][62].

**Table 2. Adsorption parameters obtained from the analysis.**

Molecule	$I_{max}/I_0$	$h_{mol}^1$ (nm)	$h_{max}$ (nm)	$A_{mol}$ (nm <sup>2</sup> )	$K_d$ (nM)	$N_S$ (nmol)	$k_{on}$ (10 <sup>3</sup> M <sup>-1</sup> s <sup>-1</sup> )	$k_{off}$ (10 <sup>-3</sup> s <sup>-1</sup> )
SBSAC deion. water	1.72	2.41	2.7	0.73	165	2.17	4.43	0.70
SBSAC buffer	1.77		2.8	0.70	163	2.79	3.51	0.57
Tween 20	1.72	2.0	2.00	0.93	372	2.33	1.86	0.69
SDS	1.03	1.77	0.45	0.97	270	1.33	8.5	2.3
Lysozyme	2.85	2.93	2.6	7.8	11.3	3.08·10 <sup>-2</sup>	107	1.21
Hexane	1.22	0.78	4.0	0.06	≥ 25200	185	≤ 0.013	0.33

<sup>1</sup>Molecular height was estimated by molecular modeling using ChemBioDraw 3D.